Nanoscale

Cite this: *Nanoscale*, 2012, **4**, 5148

www.rsc.org/nanoscale

PAPER

A facile route to fabricate an anodic TiO_2 nanotube–nanoparticle hybrid structure for high efficiency dye-sensitized solar cells†

Jia Lin,[ab] Xiaolin Liu,[a] Min Guo,[b] Wei Lu,[b] Guoge Zhang,[bc] Limin Zhou,[d] Xianfeng Chen*[a] and Haitao Huang*[b]

Received 23rd May 2012, Accepted 19th June 2012
DOI: 10.1039/c2nr31268a

The relatively low internal surface area of anodized TiO_2 nanotube arrays (TNAs) limits dye adsorption and light capturing in TNA-based dye-sensitized solar cells (DSSCs). Here, water treatment of as-anodized TNAs at room temperature was used to tailor the geometry of TNA walls in a controllable way, leading to a hybrid tube wall structure with the outer shell in a tubular morphology and the inner surface consisting of small particles. To enable front-side illumination in DSSCs, the TNAs with porous inner walls were transferred to transparent conductive oxide substrates by a self-detaching and transfer technique. The roughened water-treated TNAs show significantly enhanced internal surface area, leading to improved dye-loading and light-harvesting capabilities. Optimized performance was achieved after water treatment for 2 days, with a power conversion efficiency of 6.06%, increased by ~33% compared to conventional TNAs. Furthermore, the hybrid TNA nanostructure provides excellent electron transfer and recombination characteristics, thus promising for high efficiency DSSCs.

1. Introduction

Dye-sensitized solar cells (DSSCs) have attracted extensive attention as low-cost next-generation photovoltaic devices.[1,2] To improve their efficiencies and realize practical applications, dyes, redox electrolytes and nanostructured photoanode materials still remain to be optimized.[3–5] The conventional photoanode of DSSCs is a mesoporous thin film with randomly distributed TiO_2 nanoparticles (TNPs), which provides a large internal area for the adsorption of dyes as light absorbers. However, the architectural disorders and boundaries associated with numerous particles lead to relatively slow diffusion of photogenerated electrons in the nanoparticle network. To facilitate electron transport and collection, one-dimensional (1D) nanostructures have been utilized, such as nanotubes, nanowires and nanorods, which significantly alter electron transport and recombination dynamics.[6–8] TiO_2 nanotube arrays (TNAs) fabricated by electrochemical anodization of Ti feature a vertically oriented configuration, a high degree of self-ordering and controllable geometry, making them promising photoanode materials for DSSCs.[9–15] Furthermore, by using TNAs in DSSCs, the intrinsic light scattering effect and readily combined optical element with patterned tube walls can help absorb the sunlight more efficiently.[16–18] The highest conversion efficiency of DSSCs consisting of TNAs on transparent conducting oxide has reached 6.9%.[19]

For a vertically oriented TNA architecture, the tube-size of adequate length is relatively large (large inner diameters and thick tube walls), leading to low porosity. Also, TNAs synthesized in F^--containing organic electrolytes (ethylene glycol, glycerol, and dimethyl sulfoxide, *etc.*) usually feature straight tubes with compact and smooth walls.[13,20] As a result, TNAs often provide insufficient surface area for dye adsorption and thus low light harvesting capacity in comparison to sintered TNP systems, which is a factor limiting the improvement in conversion efficiency.[21,22] Numerous efforts have been made to enlarge the surface area and thus improve the solar cell efficiency. The fabrication of small diameter tubes, usually at a low voltage, suffers from the short tube lengths.[23–25] The decoration of the tube wall surface (both the inside and outside wall) by hydrolysis of $TiCl_4$ (particle size ~3 nm),[26,27] or the construction of mixed architecture by filling in the tubes with nanoparticles,[28–32] utilizes the hollow space in and between tubes, thus improving the surface area of the TNAs to a certain extent. The other complex hierarchical nanostructures, with both the nanotube and nanoparticle layers, show combined properties of tubes and

[a]*Department of Physics, The State Key Laboratory on Fiber Optic Local Area Communication Networks and Advanced Optical Communication Systems, Shanghai Jiao Tong University, Shanghai 200240, China. E-mail: xfchen@sjtu.edu.cn*
[b]*Department of Applied Physics and Materials Research Center, The Hong Kong Polytechnic University, Hung Hom, Kowloon, Hong Kong. E-mail: aphhuang@polyu.edu.hk*
[c]*School of Materials Science and Engineering, South China University of Technology, Guangzhou, China*
[d]*Department of Mechanical Engineering, The Hong Kong Polytechnic University, Hung Hom, Kowloon, Hong Kong*
† Electronic supplementary information (ESI) available. See DOI: 10.1039/c2nr31268a

particles.[33–35] The alteration of the tube walls, such as double-walled nanotubes,[36,37] or bamboo tubes with rings or ripples on the outer walls,[38,39] presents an improved performance in water splitting, photocatalysis and photovoltaics.

Here, we show a simple approach to achieve high efficiency TNA-based DSSCs with improved surface area. By immersing the as-anodized TNAs (which are amorphous) in water at room temperature, a hybrid structure can be achieved, with an outer shell in tubes and an inner shell in particles. The phase transformation and variation of tubular structure, through dissolution and precipitation processes, were also reported previously.[40,41] We applied this kind of hybrid TNAs in DSSCs with front-side illumination. The porous inner shell of the TNA walls which was composed of small particles could enhance the dye adsorption and light harvesting abilities, leading to significantly increased overall DSSC efficiency.

2. Experimental

Preparation of water-treated TNA membranes

Ti foils (0.125 mm thick, 99.7% purity, Strem Chemicals) were cleaned in acetone, methanol, and deionized water (DI water, 18.2 MΩ cm, Direct-Q3, Millipore) successively before anodization. Samples were anodized in a two-electrode setup (Ti foil anode and Pt foil cathode) in an ethylene glycol (EG, 99.5%) based electrolyte, with addition of 0.5 wt% NH_4F and 3 vol% DI water. The two-step anodization was carried out at 60 V using a computer controlled source meter (Model 2400, Keithley, USA). For the first step, the Ti substrate was electrochemically pre-treated for 0.5 h. The as-formed TNA layer was peeled off by ultrasonication in DI water, and then the textured Ti substrate was subjected to a second anodization for 1 h. After the anodization process, the samples were cleaned by ethanol and then immersed in DI water for 0–5 days at room temperature (~20 °C) before annealing. The water treated TNA samples show a certain amount of anatase phase, and were further pre-annealed at 400 °C for 2 h to increase the crystallinity, with a ramp rate of 5 °C min^{-1}. The free-standing TNA membranes were self-detached[42] from the underlying Ti metal substrate.

DSSC assembly

The detached water-treated TNA membranes were tightly adhered to the fluorine-doped tin oxide (FTO) substrate coated with a thin layer of TNPs of a thickness ~1 μm (hydrothermally prepared, ~20 nm in size) using a doctor-blade technique and then heated to 400 °C at 5 °C min^{-1} for 2 h to ensure a good electric conductivity. The dried TNA electrodes were immersed in an N719 ethanol solution (0.3 mM, Solaronix, Switzerland) at room temperature for 24 h. The counter electrodes were prepared by thermal decomposition of H_2PtCl_6–isopropanol solution on FTO glass at 380 °C for 30 min. The 25 μm thick hot melt film (SX1170, Solaronix, Switzerland) was used to seal the cells and the interspace was filled with a liquid electrolyte (1.0 M 1,2-dimethyl-3-propyl imidazolium iodide (DMPII), 0.12 M diiodine (I_2), 0.1 M lithium iodide (LiI), and 0.5 M 4-tert-butylpyridine (TBP) in 3-methoxypropionitrile (MPN)). The active area of the photoelectrode was 0.16 cm^2.

Characterizations

The morphology and structure of the TNAs were investigated by a field-emission scanning electron microscope (FESEM, FEI, Nova 230). X-ray diffraction (XRD, Rigaku 9KW SmartLab, Japan) patterns were collected for crystalline phase and size verification. The electrochemical properties of water treated TNAs with different durations in DSSCs were investigated by electrochemical impedance spectra (EIS, CHI 660C, CH Instruments, USA). The EIS data were collected at the open circuit voltage with an ac perturbation signal of amplitude 10 mV and frequency within 10^{-2} to 10^5 Hz. The surface area and pore size distribution of the TNAs were characterized by N_2 adsorption (ASAP 2020, Micromeritics Instruments, USA). Dye amounts were measured by desorption in 0.1 M NaOH aqueous solution and the absorbance was measured by a UV-vis spectrophotometer (Model UV-2550, Shimadzu, Japan). AM 1.5 G illumination (100 mW cm^{-2}) was provided by a 300 W solar simulator (Model 69911, Newport-Oriel Instruments, USA) calibrated using a silicon reference cell (NIST) equipped with a power meter.

3. Results and discussion

The as-anodized TNAs were immersed in water, and the smooth tube inner walls gradually became porous (depicted in Fig. 1). This is a simple and useful route to increase the surface roughness of TNA layers. However, after the thermal treatment of TNAs at a temperature as low as 200 °C, the water treatment could hardly induce any structure variation. In order to fabricate DSSCs in the configuration of front-side illumination to get rid of the disadvantageous absorptions,[43] the water-treated TNA membranes were detached from the substrate and transferred to FTO substrate. The tight attachment of TNA membranes to the FTO was achieved by a thin layer of TNPs (~1 μm). After water treatment, the entire membrane is no longer that flexible when compared with the as-prepared samples, which need careful handling during the membrane transfer process. It should be noted that prolonged immersion in water (three days or longer) possibly deteriorated the films which were even disintegrated into small pieces after annealing. When the originally smooth tube walls were completely turned into nanoparticles, the relatively loose structure would collapse easily, making it difficult to be detached from the Ti substrate.

The tube morphology changed greatly after water treatment for different durations. Fig. 2 shows the SEM images of the

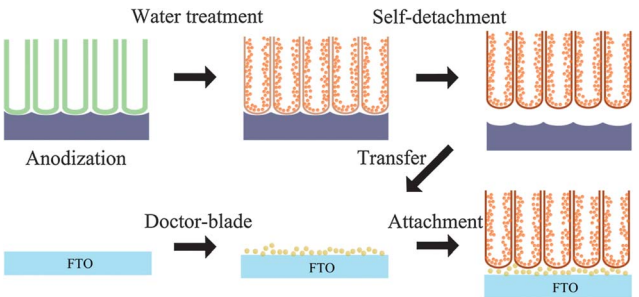

Fig. 1 Schematic illustration of the fabrication process and structure of the photoanode based on water-treated hybrid TNA membranes.

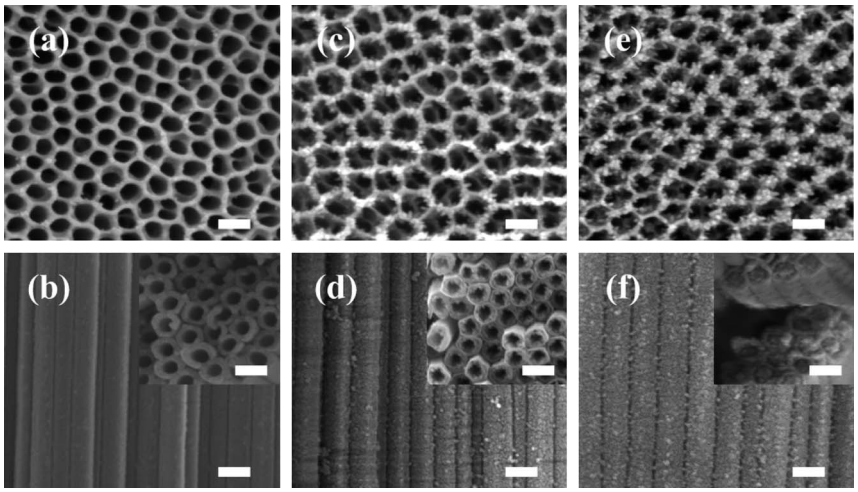

Fig. 2 Top and cross-sectional SEM images of (a and b) as-prepared TNAs by two-step anodization, and those after subsequent immersion in water at room temperature for (c and d) 2 days and (e and f) 3 days. The inset is the corresponding view of the structure underneath the top porous layer. The scale bar is 200 nm.

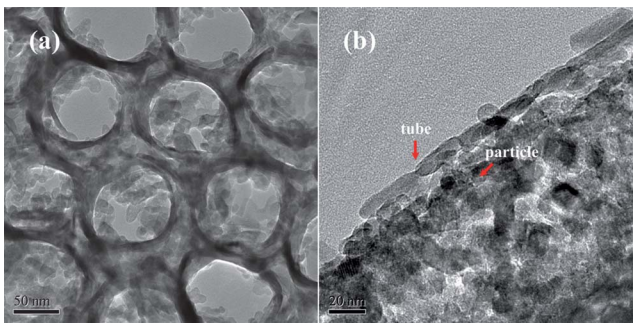

Fig. 3 TEM images of the hybrid structure with tubes and particles: (a) top view and (b) side view.

morphology evolution (0 day: without treatment, 2 days and 3 days: immersion in water for 2 and 3 days, respectively). The as-prepared TNA membrane by two-step anodization shows porous top surface and underlying smooth tube walls (Fig. 2a and b), with an outer tube diameter of ~130 nm and length of ~15 μm. For TNAs soaked in water for 1 day, no significant morphology change was observed. After 2 day water treatment, hybrid porous TNAs (with outer shell in tubes and inner shell in nanoparticles) were clearly seen (Fig. 2c and d and Fig. 3), which was more obvious for samples after 3 day water immersion (Fig. 2e and f). The sidewall consists of grains with a cylindrical shape along the tube axis with lengths of tens of nanometers (Fig. 3b), while small particles exist in the inner part, with the average crystalline size of about 11 nm. The morphology of TNAs after water treatment looked similar to tubes filled/decorated with nanoparticles.[29] However, the gradually thinning of tube sidewalls indicated that this kind of hybrid TNA was formed by consuming the tube walls and converting them to nanoparticles. In fact, the wall of TNA formed by anodization in EG usually features a double layer structure with the inner wall rich in carbon, originating from the anodization electrolyte.[44,45] Possibly due to this reason, the inner tube is easily etched by water and transformed to particles due to the different chemical

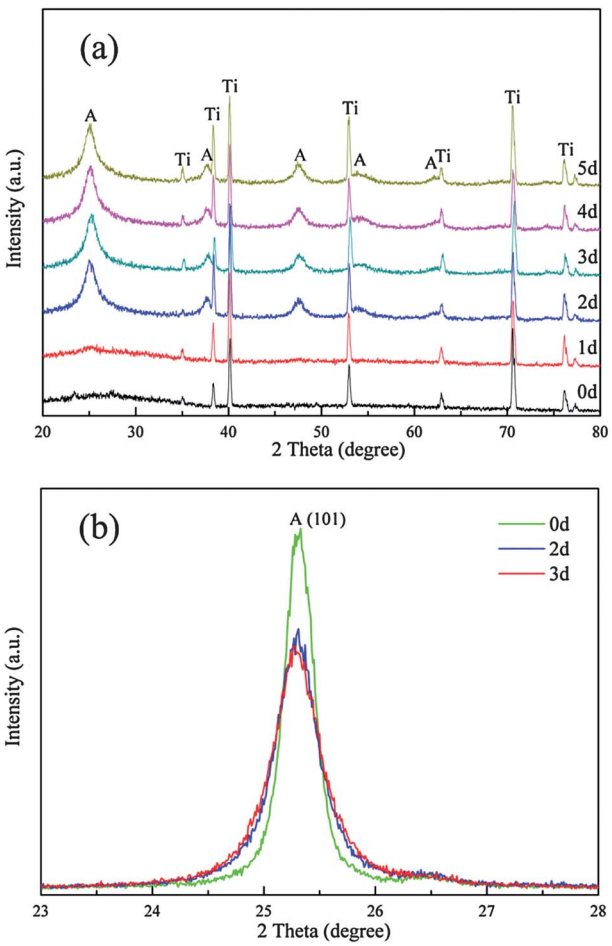

Fig. 4 (a) XRD patterns of TNAs with water treatment for 0–5 days (from bottom to top: 0 day to 5 days). A: anatase; Ti: titanium. The Ti peaks originated from the underlying substrate. (b) The detailed anatase (101) peaks of water-treated samples after the subsequent annealing process.

Table 1 Summary of the crystalline size of water-treated TNAs before and after annealing, and the average pore size of the hybrid TNA structure after annealing

Sample	Crystalline size/nm		Average pore size/nm
	Before annealing	After annealing	
0 day	—	27.0	32.7
2 days	3.8	18.7	17.3
3 days	3.9	16.6	16.5

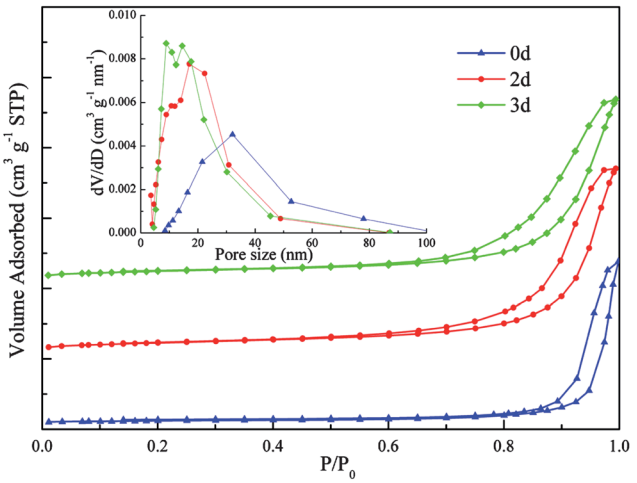

Fig. 5 The N_2 adsorption–desorption isotherm plots of the water treated TNAs. The inset shows the pore size distribution.

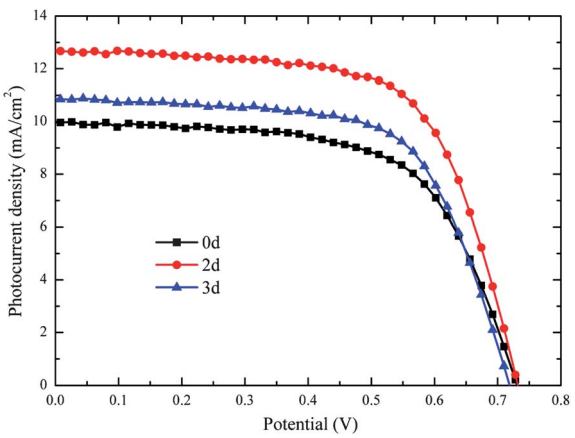

Fig. 6 The photocurrent density–voltage characteristics of DSSCs based on TNA membranes with 0 day, 2 day and 3 day water treatment.

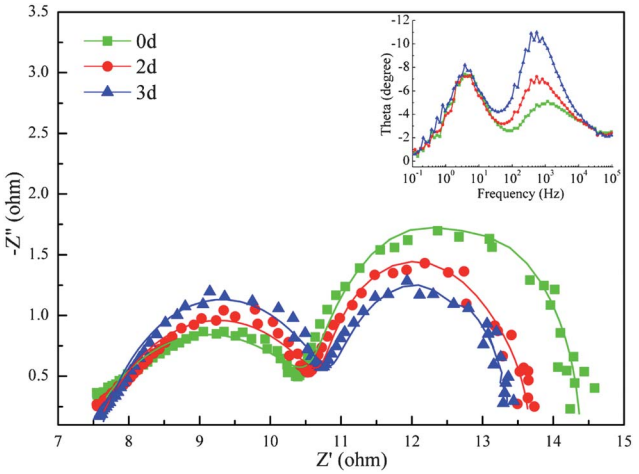

Fig. 7 Nyquist and Bode phase (inset) plots of TNAs water treated for different durations. The lines in Nyquist plots are curves fitted by the equivalent circuit.

Table 3 The detailed equivalent-circuit parameters for DSSCs based on water treated TNA membranes

Sample	R_{ct}/Ω	C_μ/mF	τ_r/ms	R_t/Ω	τ_c/ms	η_{cc} (%)
0 day	3.98	9.9	35.0	2.72	11.5	67.2
2 days	3.13	13.5	35.0	2.55	14.6	58.2
3 days	2.71	16.2	35.0	2.49	17.1	51.1

composition, similar to the etching of the tube inner part by F^- during anodization.[46] It is also noteworthy that the top surface of the untreated TNAs is smooth (Fig. 2a), while after water treatment, small nanoparticles gradually emerged on the top surface, showing rough pore mouths and a decreased pore inner diameter due to particle accumulation (Fig. 2c and e). The TNA top surface, in direct contact with water, converted to particles easily. The thinning of the tube walls and roughening of the inner surface led to the full usage of the tube inner space to increase the surface area, which was easy for dye and electrolyte infiltration. Also, the combination of tubular and particulate structure offers vectorial pathways for electron diffusion. However, further immersion in water resulted in undistinguished surface pores and underlying broken tubes (Fig. S1†) since more sidewalls were converted into particles.

The XRD patterns exhibited that after 1 day water treatment, the TNAs were still amorphous, as shown in Fig. 4a. Broad anatase peaks emerged after 2 day immersion in water, indicating that the TNAs were partially crystallized. Further elongation of the immersion duration (>2 days), however, had little

Table 2 The photovoltaic parameters of the DSSCs based on TNAs membranes immersed in water for 0 day, 2 days and 3 days and the dye amount adsorbed by the photoanodes

Sample	J_{sc}/mA cm^{-2}	V_{oc}/V	FF	η (%)	Dye adsorbed (10^{-7})/ mol cm^{-2}	BET surface area/m^2 g^{-1}
0 day	9.96	0.73	0.63	4.57	0.90 ± 0.07	20.1
2 days	12.67	0.73	0.65	6.06	1.25 ± 0.04	39.9
3 days	10.84	0.72	0.65	5.07	1.42 ± 0.13	42.7

improvement on the crystallinity of the TNAs (Fig. 4a). The small crystalline size of the TNAs, estimated from the anatase (101) peak by the Scherrer equation, reveals poor crystallinity (Table 1). The water-treated TNAs were further annealed at 400 °C in air to improve the crystallinity for application in DSSCs (Fig. 4b and Fig. S2†). After annealing, the XRD profiles show the gradual broadening of the prominent anatase (101) diffraction peaks, suggesting decreased average crystalline size with longer water treatment (from 27.0 to 16.6 nm after 3 day immersion, Table 1). As discussed above, prolonged immersion converted a larger portion of the tube walls into small particles, leading to the smaller average crystalline size of the nanotube–nanoparticle hybrid structure.

The surface area was characterized by N_2 adsorption–desorption isotherms, showing the presence of both mesopores and macropores (Fig. 5). The result shows that the Brunauer–Emmett–Teller (BET) surface areas of TNA membranes for 0 day, 2 day and 3 day water treated samples are ~20.1, 39.9 and 42.7 $m^2\ g^{-1}$ (2.1 times larger after 3 day treatment). For longer immersion, the surface area could be enlarged further.[40] The corresponding Barrett–Joyner–Halenda (BJH) pore size distribution is shown in the inset of Fig. 5. The hybrid TNA structure with coexistent macroporous tubes and mesoporous walls shows a decreased average pore size, from 32.7 to 16.5 nm after 3 day water treatment (Table 1), which is consistent with the gradually enlarged internal surface area.

The photocurrent density–voltage characteristics of DSSCs based on hybrid TNAs under AM 1.5G solar condition (100 mW cm^{-2}) are shown in Fig. 6 and detailed parameters summarized in Table 2. With the enlarged internal surface area of TNA films, the amount of dye adsorbed increased significantly by 38.9 and 57.8%, after 2 day and 3 day immersion, respectively (Table 2). The increment of dye loading is not proportional to that of surface area, which implies that not all the internal surfaces of the hybrid TNAs are accessible to dye molecules, consistent with the decreased pore size after water treatment (inset of Fig. 5). As a result of increased dye loading, the short-circuit current density (J_{sc}) increased from 9.96 to 12.67 mA cm^{-2} after 2 day water treatment (increased by 27.2%). However, for 3-day tubes, J_{sc} decreased to 10.84 mA cm^{-2}. For TNAs with different immersion duration, the open-circuit voltage (V_{oc}) and the fill factor (FF) remained almost unchanged. Thus, the DSSCs based on TNAs immersed in water for 2 days show the best overall solar energy conversion efficiency (η) of 6.06%, a ~33% increase compared to samples based on untreated TNAs. A further increase in the duration of water treatment was disadvantageous (resulting in a lower J_{sc}, with $\eta = 5.07\%$), as will be discussed in detail below.

The electrochemical properties of the DSSCs were analyzed by electrical impedance spectroscopy (EIS) under open-circuit conditions. The Nyquist curves were fitted according to the equivalent circuit model (Fig. 7, the details are provided in ESI†), and the derived parameters are shown in Table 3. The diameter of the medium-frequency semicircles decreased obviously for longer water immersion duration, denoting the reduced charge transfer resistance (R_{ct}) at the TiO_2/dye/electrolyte interfaces.[47,48] The lower interfacial resistance of electron transfer from the dye to TNAs is due to the enlarged surface area and also the efficient electrolyte diffusion in the hybrid TNA structure. The larger surface area after water treatment also results in the increased surface trap states for electrons, thus leading to a larger chemical capacitance (C_μ) of the photoanode.[49] The C_μ increased by 63.6% for 3 days water treated TNAs, consistent with the increment of the amount of dye loading. As the transport resistance (R_t) changed only slightly, the larger C_μ leads to a longer electron transport time (τ_c) in the photoanode, resulting in lower electron collection efficiency (η_{cc}). Thus with gradually enlarged surface area, the lower electron collection competed with the greater light harvesting and eventually a lower overall conversion efficiency was obtained after prolonged water treatment of 3 days. Moreover, as mentioned above, the TNA film quality also gradually decreased with the appearance of broken outer tube walls, leading to collapsed tube architecture. The electron lifetime (τ_r) was calculated from the Bode phase plots shown in the inset of Fig. 7 by $\tau_r = 1/(2\pi f_{peak})$, where f_{peak} is the frequency of the characteristic peak in the mid-frequency (1–100 Hz) region.[50] The lifetime for 0 day, 2 day and 3 day treated samples is almost the same (~35.0 ms, Table 3), showing a similar recombination property. It has been observed that the lifetime of photogenerated electrons in TNAs is much longer than that in sintered TNPs (~10 times),[16,51,52] and the TNAs decorated with nanoparticles featured decreased lifetimes.[29,30] In contrast, the water-treated hybrid films have the same low electron recombination probability as the TNA systems, resulting in an efficient electron collection.

4. Conclusion

In above work, simple modification of the TNA surface area was achieved by water treatment with a nanotube–nanoparticle hybrid structure. The water treated TNAs were incorporated into front-side illuminated DSSCs, exhibiting a greatly enhanced solar energy conversion efficiency of 6.06% (improved by ~33%). The improved solar cell performance is primarily due to the enlarged surface area with increased dye-loading and light-harvesting capacity. Also, the hybrid structure exhibited low electron transfer resistance and comparatively slow recombination. These results inspire a facile approach to the fabrication of TNAs with large surface areas for DSSC applications.

Acknowledgements

The work was supported by the grants received from the Research Grants Council of the Hong Kong Special Administrative Region (PolyU5187/09E and PolyU5349/10E) and the Hong Kong Polytechnic University (A-SA76). It was also supported by the National Natural Science Foundation of China (Grant no. 61125503) and the Foundation for Development of Science and Technology of Shanghai (Grant no. 11XD1402600, no. 10JC1407200).

References

1 B. O'Regan and M. Grätzel, *Nature*, 1991, **353**, 737–740.
2 B. E. Hardin, H. J. Snaith and M. D. McGehee, *Nat. Photonics*, 2012, **6**, 162–169.
3 J. M. Kroon, N. J. Bakker, H. J. P. Smit, P. Liska, K. R. Thampi, P. Wang, S. M. Zakeeruddin, M. Grätzel, A. Hinsch and S. Hore, *et al.*, *Progr. Photovolt.: Res. Appl.*, 2007, **15**, 1–18.

4 A. Yella, H. W. Lee, H. N. Tsao, C. Yi, A. K. Chandiran, M. K. Nazeeruddin, E. W. G. Diau, C. Y. Yeh, S. M. Zakeeruddin and M. Grätzel, *Science*, 2011, **334**, 629–634.
5 I. Chung, B. Lee, J. He, R. P. H. Chang and M. G. Kanatzidis, *Nature*, 2012, **485**, 486–489.
6 C.-T. Yip, M. Guo, H. Huang, L. Zhou, Y. Wang and C. Huang, *Nanoscale*, 2012, **4**, 448–450.
7 S. H. Kang, S. H. Choi, M. S. Kang, J. Y. Kim, H. S. Kim, T. Hyeon and Y. E. Sung, *Adv. Mater.*, 2008, **20**, 54–58.
8 M. Adachi, Y. Murata, J. Takao, J. Jiu, M. Sakamoto and F. Wang, *J. Am. Chem. Soc.*, 2004, **126**, 14943–14949.
9 G. K. Mor, K. Shankar, M. Paulose, O. K. Varghese and C. A. Grimes, *Nano Lett.*, 2006, **6**, 215–218.
10 P. Roy, D. Kim, K. Lee, E. Spiecker and P. Schmuki, *Nanoscale*, 2010, **2**, 45–59.
11 D. Kuang, J. Brillet, P. Chen, M. Takata, S. Uchida, H. Miura, K. Sumioka, S. M. Zakeeruddin and M. Grätzel, *ACS Nano*, 2008, **2**, 1113–1116.
12 K. Shankar, J. Bandara, M. Paulose, H. Wietasch, O. K. Varghese, G. K. Mor, T. J. LaTempa, M. Thelakkat and C. A. Grimes, *Nano Lett.*, 2008, **8**, 1654–1659.
13 K. Shankar, G. K. Mor, H. E. Prakasam, S. Yoriya, M. Paulose, O. K. Varghese and C. A. Grimes, *Nanotechnology*, 2007, **18**, 065707.
14 G. K. Mor, O. K. Varghese, M. Paulose, K. Shankar and C. A. Grimes, *Sol. Energy Mater. Sol. Cells*, 2006, **90**, 2011–2075.
15 V. Galstyan, A. Vomiero, I. Concina, A. Braga, M. Brisotto, E. Bontempi, G. Faglia and G. Sberveglieri, *Small*, 2011, **7**, 2437–2442.
16 K. Zhu, N. R. Neale, A. Miedaner and A. J. Frank, *Nano Lett.*, 2007, **7**, 69–74.
17 J. Lin, K. Liu and X. F. Chen, *Small*, 2011, **7**, 1784–1789.
18 C.-T. Yip, H. T. Huang, L. M. Zhou, K. Y. Xie, Y. Wang, T. H. Feng, J. Li and W. Y. Tam, *Adv. Mater.*, 2011, **23**, 5624–5628.
19 O. Varghese, M. Paulose and C. Grimes, *Nat. Nanotechnol.*, 2009, **4**, 592–597.
20 J. M. Macak, H. Tsuchiya, L. Taveira, S. Aldabergerova and P. Schmuki, *Angew. Chem., Int. Ed.*, 2005, **44**, 7463–7465.
21 E. Ghadiri, N. Taghavinia, S. M. Zakeeruddin, M. Grätzel and J. E. Moser, *Nano Lett.*, 2010, **10**, 1632–1638.
22 T. Kang, A. Smith, B. Taylor and M. Durstock, *Nano Lett.*, 2009, **9**, 601–606.
23 J. Park, S. Bauer, K. von der Mark and P. Schmuki, *Nano Lett.*, 2007, **7**, 1686–1691.
24 N. Liu, K. Lee and P. Schmuki, *Electrochem. Commun.*, 2012, **15**, 1–4.
25 J. Park, S. Bauer, K. A. Schlegel, F. W. Neukam, K. von der Mark and P. Schmuki, *Small*, 2009, **5**, 666–671.
26 P. Roy, D. Kim, I. Paramasivam and P. Schmuki, *Electrochem. Commun.*, 2009, **11**, 1001–1004.
27 C. C. Chen, H. W. Chung, C. H. Chen, H. P. Lu, C. M. Lan, S. F. Chen, L. Y. Luo, C. S. Hung and E. W. G. Diau, *J. Phys. Chem. C*, 2008, **112**, 19151–19157.
28 C. Rho and J. S. Suh, *Chem. Phys. Lett.*, 2011, **513**, 108–111.
29 X. Pan, C. H. Chen, K. Zhu and Z. Y. Fan, *Nanotechnology*, 2011, **22**, 235402.
30 S. H. Wang, J. B. Zhang, S. Chen, H. T. Yang, Y. Lin, X. R. Xiao, X. W. Zhou and X. P. Li, *Electrochim. Acta*, 2011, **56**, 6184–6188.
31 M. D. Ye, X. K. Xin, C. J. Lin and Z. Q. Lin, *Nano Lett.*, 2011, **11**, 3214–3220.
32 Y. Alivov and Z. Fan, *Appl. Phys. Lett.*, 2009, **95**, 063504.
33 Q. Zheng, H. Kang, J. Yun, J. Lee, J. H. Park and S. Baik, *ACS Nano*, 2011, **5**, 5088–5093.
34 H. G. Yun, J. H. Park, B. S. Bae and M. G. Kang, *J. Mater. Chem.*, 2011, **21**, 3558–3561.
35 X. K. Xin, J. Wang, W. Han, M. D. Ye and Z. Q. Lin, *Nanoscale*, 2012, **4**, 964–969.
36 S. E. John, S. K. Mohapatra and M. Misra, *Langmuir*, 2009, **25**, 8240–8247.
37 X. J. Xu, X. S. Fang, T. Y. Zhai, H. B. Zeng, B. D. Liu, X. Y. Hu, Y. Bando and D. Golberg, *Small*, 2011, **7**, 445–449.
38 D. Kim, A. Ghicov, S. P. Albu and P. Schmuki, *J. Am. Chem. Soc.*, 2008, **130**, 16454–16455.
39 S. P. Albu, D. Kim and P. Schmuki, *Angew. Chem., Int. Ed.*, 2008, **47**, 1916–1919.
40 D. A. Wang, L. F. Liu, F. X. Zhang, K. Tao, E. Pippel and K. Domen, *Nano Lett.*, 2011, **11**, 3649–3655.
41 Y. L. Liao, W. X. Que, P. Zhong, J. Zhang and Y. C. He, *ACS Appl. Mater. Interfaces*, 2011, **3**, 2800–2804.
42 J. Lin, J. F. Chen and X. F. Chen, *Electrochem. Commun.*, 2010, **12**, 1062–1065.
43 J. Y. Kim, J. H. Noh, K. Zhu, A. F. Halverson, N. R. Neale, S. Park, K. S. Hong and A. J. Frank, *ACS Nano*, 2011, **5**, 2647–2656.
44 S. P. Albu and P. Schmuki, *Phys. Status Solidi RRL*, 2010, **4**, 215–217.
45 S. P. Albu, A. Ghicov, S. Aldabergenova, P. Drechsel, D. LeClere, G. E. Thompson, J. M. Macak and P. Schmuki, *Adv. Mater.*, 2008, **20**, 4135–4139.
46 S. Berger, H. Tsuchiya and P. Schmuki, *Chem. Mater.*, 2008, **20**, 3245–3247.
47 L. Y. Han, N. Koide, Y. Chiba and T. Mitate, *Appl. Phys. Lett.*, 2004, **84**, 2433–2435.
48 M. Adachi, M. Sakamoto, J. Jiu, Y. Ogata and S. Isoda, *J. Phys. Chem. B*, 2006, **110**, 13872–13880.
49 K. Zhu, N. Kopidakis, N. R. Neale, J. van de Lagemaat and A. J. Frank, *J. Phys. Chem. B*, 2006, **110**, 25174–25180.
50 R. Kern, R. Sastrawan, J. Ferber, R. Stangl and J. Luther, *Electrochim. Acta*, 2002, **47**, 4213–4225.
51 J. R. Jennings, A. Ghicov, L. M. Peter, P. Schmuki and A. B. Walker, *J. Am. Chem. Soc.*, 2008, **130**, 13364–13372.
52 C. K. Xu, P. H. Shin, L. L. Cao, J. M. Wu and D. Gao, *Chem. Mater.*, 2010, **22**, 143–148.